JOURNAL OF MATERIALS SCIENCE 39 (2004) 4271–4286

Effect of cationic substituents on particle morphology of goethite and the magnetic properties of maghemite derived from substituted goethite

C. SUDAKAR, G. N. SUBBANNA†, T. R. N. KUTTY*
Materials Research Centre, Indian Institute of Science, Bangalore 560012, India
E-mail: kutty@mrc.iisc.ernet.in

Preparation of nanoparticles with the desired shape and size by the wet-chemical precipitation process is a challenging task. Thus, the effects of different substitutional impurities such as Al, Cr, Co or Ni on the particle morphology and phase stability of goethite have been investigated. Goethite is prepared by air oxidation of $Fe(OH)_2 \cdot xH_2O$ gel under near neutral conditions. Below certain concentration levels of dopants ($Al^{3+} \leq 10$; $Cr^{3+} \leq 5$; $Co^{2+} \leq 10$ and $Ni^{2+} \leq 5$ at.%) the samples remained monophasic as revealed by XRD, TEM, and IR studies. Above these levels, the substituents produce traces of secondary phases such as lepidocrocite, spinel ferrite and $M^n(OH)_n$. The goethite structure is stable in spite of the iso- or aliovalent substitutions. The individual additives have divergent influence on the particle morphology; Al^{3+} and Cr^{3+} decreases the particle size to $<$50 nm and aspect ratio (AR) $<$2. Co-substitution produces slender particles with AR as high as 25. Whereas, Ni^{2+} does not have any influence on the particle morphology. The attributable factors in morphology control are the increased nucleation rate, restricted growth along needle axes, and the strain induced in the goethite lattice as a result of difference in ionic radii. Maghemite, γ-$Fe_2O_{3-\delta}$, particles are obtained from goethite wherein the topotactic conversion renders the retention of the particle morphology of the precursor. Maghemite with substituted impurities showed substantial differences in magnetic properties. Saturation magnetization (σ_s) and coercivity (H_c) go down to very low values due to relaxation of spins on the surface atoms as revealed by Mössbauer spectroscopy. Decrease in coercivity is by way of the presence of diamagnetic ion (Al^{3+}). Whereas, Co-substituted maghemite has enhanced H_c as a result of high magnetocrystalline anisotropy accompanied by the shape anisotropy.

1. Introduction

Much attention has been focused on the approach of particle size and shape control by growth-directed processes typical of precipitation methods. The synthesis conditions can control the morphology of the particles, while the effect of additives and impurities (both anionic and cationic) remain obscure [1]. One such system of industrial importance is goethite, α-FeOOH, which is an important precursor for γ-$Fe_2O_{3-\delta}$ particulate magnetic recording media. It also finds applications in preparing materials employed as catalysts, anticorrosion paints, abrasive materials, magnetic oxide ceramics, gas sensors, etc. [2]. The properties of these particles depend not only on the composition but also crucially on the size and shape. For example, for acicular maghemite (γ-$Fe_2O_{3-\delta}$) used as magnetic powder in recording information, the length/width ratio of the particles must be higher than 10 [3]. Commercially applied route also uses hematite precursor particles instead of FeOOH [4]. However, most of these particles are "rice-shaped" with aspect ratio around 3 to 5. The maghemite particles obtained from this process are polycrystalline in nature. As maghemite belongs to cubic crystal system with spinel structure (as also magnetite), it is not possible to precipitate it directly in a needle-like shape. Thus, the synthesis has been done through the topotactic transformation of another solid precursor such as α- or γ-FeOOH. The morphological properties of iron oxide particles depend on the competition between the processes (such as nucleation, growth, aggregation, and impurity adsorption) that control the development of a solid particle from a

†Deceased on 16th July 2003.
*Author to whom all correspondence should be addressed.

solution. The dominant influence of one of these factors in the final morphological properties will depend on variables such as pH, temperature, initial concentration of reagents as well as $[Fe^{2+}]/[OH^-]$ ratio, the nature of anions present, and the rate of oxidation. The importance of size and morphology is not restricted to iron oxides [1]. It is a general characteristic of metal oxide powders used for a variety of applications, and justifies the special attention extended to synthetic procedures that allow close control of particle shape. High demand of particles for magnetic applications with narrow distribution of size and shape has kept the studies on the preparation conditions and property optimization of goethite a vibrant field. Thus, the formation and stability of goethite together with acicular shape, aspect ratio and the desired size of the particles depend on the factors mentioned above. The commonly used methods of preparation for goethite are alkaline or near-neutral processes [4]. Although well-grown crystalline particles are readily obtained in alkaline media, the time and processing difficulties involved in the preparation are unrealizable [5, 6]. Processes carried out under near-neutral conditions do give rise to crystalline particles of acicular goethite under controlled precipitation and oxidation in presence of morphology controlling cationic additives [7]. However, presence of structurally retained water molecules is inevitable, giving rise to hydrogoethite, which is physically similar to goethite except for the excess water of hydration [8]. Presence of trace anionic or cationic impurities tremendously affects the stability of the phase and particle size, which has been scarcely noticed. Further, synthetic goethite prepared under highly alkaline conditions incorporates isovalent (Al^{3+}, Cr^{3+}, V^{3+}, Mn^{3+} etc.) as well as aliovalent impurity cations (Ni^{2+}, Co^{2+}, Zn^{2+}, Cd^{2+}, etc.) into its structure [6]. Aluminium ions can be incorporated in relatively high proportions (upto 33 mol%) by isomorphous substitution of Fe^{3+} in the octahedral sites of goethite structure. However the effects of these substituent impurities on the crystallinity and particle size are unclear in the near-neutral process. In the present work we report the influence of some of the metal cations (Al^{3+}, Cr^{3+}, Ni^{2+} and Co^{2+}) on the formation, phase stability, shape and size of goethite particles. The magnetic properties of maghemite (γ-$Fe_2O_{3-\delta}$) formed from the substituted goethite have also been investigated.

2. Experimental

Acicular goethite particles were prepared by air oxidation of aqueous suspensions of $Fe(OH)_2{\cdot}xH_2O$ ($80 < x < 120$). NH_4OH (aq) (1M) solution added in aliquots of 20–25 ml at regular intervals of 1–1.5 h was used to precipitate $Fe(OH)_2{\cdot}xH_2O$ from ferrous ammonium sulphate (FAS) solution (0.1 M) in presence of morphology controlling cationic additive (0.01 at.% of Pd^{2+} from $Pd(NH_3)_6Cl_2$) at room temperature (25°C). A detailed study on the preparative conditions and characteristics of the resulting goethite particles was presented elsewhere [7]. The precipitated goethite particles were washed with distilled water, dried in oven (∼100°C) and then dispersed sonically in acetone or ethanol followed by filtration and drying.

The effect of substituents such as isovalent (Al^{3+}, Cr^{3+}) and aliovalent (Ni^{2+}, Co^{2+}) cations for Fe^{3+} on the morphological features [crystallite size and aspect ratios (AR) distribution] and phase purity of the particles were also studied. The metal ion (M^{n+}) substituted goethite with $100\,M/[M + Fe] = 0$ to 20 at.% were prepared from the mixed solutions of FAS and M^{n+} salt (sulphate). The other conditions of preparation were maintained the same as those used for goethite. Representative examples of substituted goethite, given in Table I, are designated as HG-Mx (where Mx is 'x' at.% of metal cation, M^{n+}, substituted in goethite). In order to understand the changes in magnetic properties of γ-$Fe_2O_{3-\delta}$ under the influence of different substitutions, particle size and aspect ratio, substituted goethite were reduced in H_2 atmosphere at 270°C to obtain magnetite. The latter was further air oxidized at 270°C to derive the substituted maghemite. Representative samples are characterized for its microstructural and magnetic properties. The samples are labeled as ROHG-Mx where R and O indicate the reduction (R) followed by oxidation (O) of HG-Mx carried out as two different steps.

X-ray powder diffractograms of the goethite samples were obtained from a Scintag (USA) diffractometer equipped with copper X-ray tube and a diffracted-beam monochromator at a scanning rate of $0.2^\circ\ 2\theta$/min. The samples were mixed with polysilicon as the internal standard. The unit cell dimensions were calculated from the corrected positions of at least 10 XRD lines using least square procedures without weighting the reflections with respect to theta. The weight losses and dehydroxylation temperatures of the substituted goethite were studied by thermal analyses using

TABLE I Composition of substituted goethite samples dried at 120°C

Sample identity	Substitution concentration $100 * M/(M + Fe)$ at.%	Theoretical weight loss $2Fe_{1-x}M_x^{n+}O(OH)_{1+(n-3)x} \rightarrow Fe_{2(1-x)}M_{2x}^{n+}O_{3+(n-3)x}$	Isothermal weight loss (at 900°C)	Composition of substituted HG $Fe_{1-x}M_x^{n+}O(OH)_{1+(n-3)x}{\cdot}yH_2O$
HG	0	10.13	13.77	$FeO(OH).\ (H_2O)_{0.208}$
HG-Al0.4	0.4	10.14	13.60	$Fe_{0.996}Al_{0.004}O(OH){\cdot}(H_2O)_{0.197}$
HG-Al2	2	10.20	13.99	$Fe_{0.98}Al_{0.02}O(OH){\cdot}(H_2O)_{0.216}$
HG-Al 9	9	10.44	14.12	$Fe_{0.91}Al_{0.09}O(OH){\cdot}(H_2O)_{0.209}$
HG-Co5	5	9.70	13.1	$Fe_{0.95}Co_{0.05}O(OH)_{0.95}{\cdot}(H_2O)_{0.192}$
HG-Co10	10	9.26	12.2	$Fe_{0.90}Co_{0.10}O(OH)_{0.90}{\cdot}(H_2O)_{0.162}$
HG-Cr5	4.76	10.15	13.02	$Fe_{0.952}Cr_{0.048}O(OH){\cdot}(H_2O)_{0.162}$
HG-Ni5	4.76	9.72	11.61	$Fe_{0.952}Ni_{0.048}O(OH)_{0.952}{\cdot}(H_2O)_{0.105}$

a simultaneous thermogravimetry/differential thermal analyzer (TG-DTA), Polymer Laboratory, STA 1500, at a heating rate of 5°C/min, in air. Weight loss measurements were also carried out by heating the samples under isothermal conditions at selected temperatures. The evidence of lattice substitutions of M^{n+} cations were obtained from the infrared absorption spectra of substituted goethite recorded on a Perkin-Elmer spectrometer in the range of 4000 to 400 cm^{-1} by dispersing the samples in anhydrous KCl pellets. The evidence of substitution was also obtained from the change in the unit cell dimensions as indicated by X-ray diffraction analyses. Core-level X-ray photoelectron spectra of the samples were recorded using Al Kα incident X-rays on a Vaccuum Generators ESCA 3 Mk II instrument. Morphological studies were carried out with a Jeol JEM 200CX, transmission electron microscope (TEM). Particle sizes and shapes were evaluated by the intercept methods from the micrographs. To study the magnetization with respect to the applied field, pressed pellets of the samples were subjected to magnetic measurements using a vibrating sample magnetometer (VSM, Lakeshore, USA). Mössbauer spectra were recorded at constant acceleration in conjunction with a Nuclear Data Instruments ND60 multichannel analyzer using a ^{57}Co source in rhodium matrix. The experimentally observed Mössbauer spectra were curve-fitted by a least-squares method by computer [9], assuming Lorentzian line shapes.

3. Results

3.1. XRD studies

Fig. 1 shows the X-ray diffraction patterns of undoped as well as substituted goethites indicating that the samples are monophasic, notwithstanding the fact that the substitutions of metal ions are in high concentrations. Sample HG shows crystalline X-ray diffraction pattern corresponding to that of phase-pure goethite (α-FeOOH), having the space group Pbnm. However, marginal increase in '*a*' and '*b*' lattice parameters was observed, while the *c*-axis remaining close to that of the reported value of 3.015 Å [10]. With increasing Al^{3+} substitution (Fig. 1a), the peak width at half maximum (FWHM) increases as a result of decrease in particle size. With Cr^{3+}, Co^{2+} or Ni^{2+} substitutions, the goethite phase does not transfer into akaganéite or lepidocrocite (β or γ-FeOOH). Whereas discernible peak broadening is observed for HG-Cr5 and HG-Co10 samples (Fig. 1b). Further, slight shifts in the peak positions have been observed in all the substituted samples which indicate the changes in the lattice parameters. The lattice parameters of these samples with the variations in concentration of the substituents are shown in Fig. 2. Goethite (HG) shows increased '*a*' and '*b*' parameters due to residually retained water molecules located in the strands of channels formed in-between the double ribbons of $Fe(O,OH)_6$ octahedra running parallel to the *c*-axis [7]. The lattice parameters decrease considerably with increasing mole ratio of Al^{3+}, Cr^{3+} or Co^{2+} substituted HG (Fig. 2). The decrease was minimum in the case of Ni^{2+}-substituted HG. The congruent decrease in *a*, *b* and *c* parameters due to the effect of the alio- or iso-valent substituents can be explained by structural considerations and crystallochemical properties of the incorporated metal ions. Systematic decrease of the unit-cell dimensions with increasing substitution of Al^{3+} is related to the ionic radius of Al^{3+} ($r = 0.53$ Å; VI-coordinated, S-P value [11]), which is smaller than the ionic radius (high spin) of Fe^{3+} ion ($r = 0.645$ Å). The lattice parameters of Al^{3+} substituted HG (HG-Alx) does not follow the linear relationship (Vegard's rule). At low concentrations (<2 at.%), the lattice parameter decreases rapidly whereas with >2 at.% of Al^{3+} the changes are nearly linear with lower slopes. In the case of Cr^{3+} (HG-Cr5), the changes in lattice parameters are smaller, because the ionic radius of Cr^{3+} ion ($r = 0.615$ Å) is close to that of Fe^{3+}. The lattice parameter decreases linearly with Cr^{3+} concentration. For HG-Ni, the lattice parameters decrease despite the larger ionic radius of Ni^{2+} ($r = 0.7$ Å) over Fe^{3+}. This can be due to the anionic defect created to charge

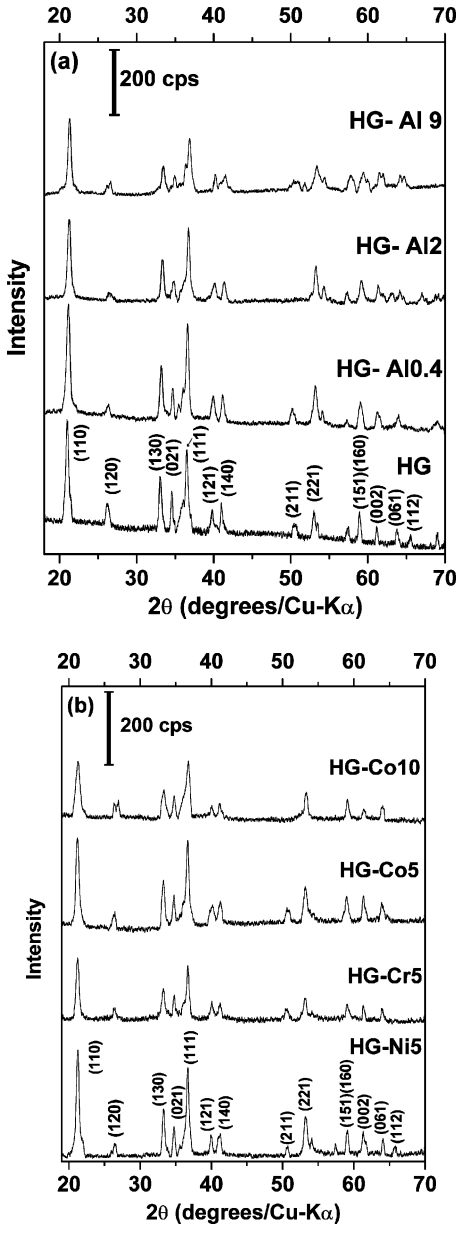

Figure 1 (a) XRD patterns of Al^{3+}-substituted goethite samples (HG-Al*x*; $x = 0, 0.4, 2$ and 9). (b) XRD patterns of HG-Ni5, HG-Cr5, HG-Co5 and HG-Co10.

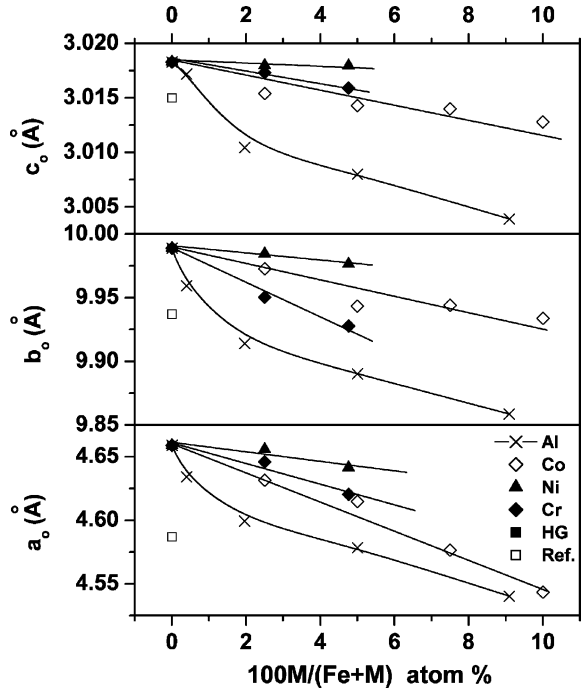

Figure 2 Unit cell lattice dimension (a_0, b_0, and c_0) as a function of x at.% substitution for different substituent ions in goethite.

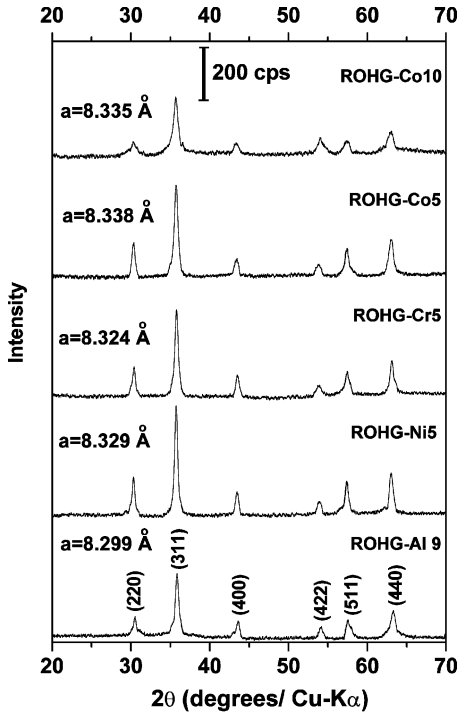

Figure 3 XRD patterns of maghemite (ROHG-Al 9, ROHG-Ni5, ROHG-Cr5, ROHG-Co5 and ROHG-Co10) derived from substituted goethite.

compensate the presence of Ni^{2+} in place of Fe^{3+}. With Co^{2+} ($r = 0.74$ Å; high spin) the decrease was more pronounced when compared to that of HG-Ni. This implies that Co ion exists in 3+ state ($r = 0.61$ Å) in the lattice. The incorporation of Co^{2+} into the goethite structure is preceded by the oxidation of the Co to the trivalent form, thus showing pronounced decrease in lattice parameters. Though the anion (O^{2-}/OH^-) vacancies need not always show noticeable decrease in cell parameters, diminished amount of bridging H_2O may be the other reason. This also accounts for the deviation from linearity (Vegard's rule) of lattice parameter with increasing concentration of substituents. It is evidenced from the isothermal weight loss measurements that Ni^{2+}/Co-substituted HG shows lower weight losses compared to Al^{3+}/Cr^{3+} substituted HG (Table I). The possibility of Ni^{3+} ($r = 0.6$ Å; high spin) or Co^{3+} ($r = 0.61$ Å; high spin) formation during aeration has been carried out by studying the oxidation states of Co and Ni using core-level X-ray photoelectron spectroscopy (XPS) (see the Section 3.2). Though XPS study shows both these ions in 2+ state, it is more representative of the atoms on the surface (∼20–30 Å) of the particles. Therefore the oxidation state of the substitutional atoms cannot be precisely determined by this technique. Thus, the lattice parameter varies with the concentration of substituents and the crystal chemistry of the cations (iso- or alio-valent). The effect of residually retained water molecules on the 'a_o' and 'b_o' parameters is also considerable.

X-ray diffraction patterns of maghemite samples obtained from substituted HG along with the observed lattice parameter 'a' of the defect spinel are presented in Fig. 3. It shows slight decrease compared to $a = 8.35$ Å for the unsubstituted γ-$Fe_2O_{3-\delta}$. The relative intensities as well as the line widths of X-ray reflections show differences between the samples; e.g., the intensities of Co and Al substituted samples are lower compared to Ni and Cr containing goethite. The average crystal size obtained from corrected XRD line width of (311) peak using the Scherrer formula shows mean coherence length ($MCL_{(311)}$) of ∼10–12 nm for ROHG-Co10 and ROHG-Al 9, while that of the other samples is around 16–20 nm. Such low mean coherence length obtained from X-ray line broadening may arise due to multiple contributions from particle size and shape, defects including mesopores, dislocations and point defects. Notwithstanding the large differences in aspect ratio from 2 to 25, the MCL of 10 to 20 nm cannot be explained on the basis of shape factors. Further, the particles are free from dislocations and point defects as observed from the high-resolution images by electron microscopy. Thus, the near uniform distribution of mesopores in the particle gives rise to the apparent size of 10 to 20 nm by X-ray line broadening, which is smaller than the actual length or width of the particles.

3.2. X-ray photoelectron spectroscopy

The oxidation state of Co in HG-Co5 and Ni in HG-Ni5 samples is established using core-level X-ray photoelectron spectroscopy (XPS). Co2p and Ni2p core level spectra of the respective samples are shown in Fig. 4. The positions of the peaks in the spectra are adjusted for sample charging by using the C1s signal at 285 eV as the reference. The $2p_{3/2}$ and $2p_{1/2}$ binding energies (BE) for Co are 781.2 and 796.6 eV respectively. However, Co^{2+} cannot be distinguished from Co^{3+} from the binding energies of the 2 p levels (chemical shift) nor by spin orbit splitting value, ΔE = BE $2p_{1/2}$ − BE $2p_{3/2}$, which reflects the overall electron density. However, the electronic configuration of 3d levels in Co can be recognized from the satellite structures which originate from the shake-up process involving the 3d →

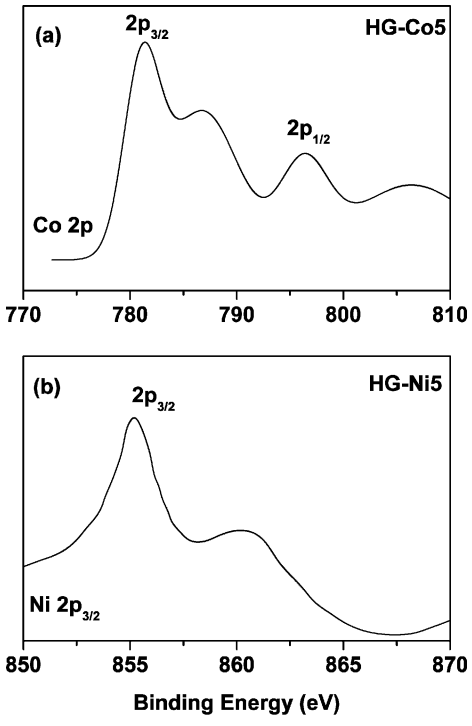

Figure 4 XPS spectra of (a) Co(2p) levels in HG-Co5 and (b) Ni(2p) levels in HG-Ni5.

4s transition, and are only influenced by the strongly covalent bonding ligands. Similar way of distinction between Ni^{2+} and Ni^{3+} are used, wherein for the lower oxidation state, Ni (2p) are associated with the intrinsic satellite structure. The pronounced intensities of the satellites in Fig. 4a shows that the Co species is in lower oxidation state. Although this is identified from the satellite peaks, the main peaks can comprise of both Co^{2+} and Co^{3+} contributions. Further the spectral details are more representative of the atoms lying on the surface (∼20–30 Å) of the particles. The substituents in the core of the particles are not clearly inferred from this technique. Ni in the sample HG-Ni5 also exists in 2+ state (Fig. 4b) with Ni $2p_{3/2}$ appearing at 855.2 eV with the corresponding intrinsic satellite structures. However the peak intensities are very low because of the lower concentrations of the substituent species in the samples.

3.3. TEM studies

To understand the effect of substituents on the particle morphology, studies were carried out using transmission electron microscopy (TEM). TEM micrographs of substituted HG particles are shown in Figs 5 and 6. The length as well as the aspect ratio (AR) distributions of these particles was measured (Table II). The corresponding histograms for the case of HG-Alx are shown in Fig. 7, which are constructed from measurements of over 300 particles in each case. It is clear that the distribution of length as well as the AR decreases noticeably with the concentration of Al^{3+} (Figs 5 and 7). For the undoped HG, the particle lengths varied from 200 to 400 nm with AR maximizing around 9. With the increase in Al^{3+}-substitution, the average particle length decreases, e.g. ∼50 nm for 9 at.% Al^{3+}. The distribution curves are very narrow in comparison to that of undoped goethite. The AR is the smallest for Cr- and largest for Co-substituted samples, with the average particle lengths around 50, 250, and 400 nm for HG-Cr5, HG-Ni5 and HG-Co5 respectively. The distribution of particle length as well as AR remains unchanged with higher Co concentrations (>5 at.%). The AR extends up to 25 for Co-substituted HG. It is also observed that with high concentrations of Co-substitution, acicular particles exist as aggregates. Such aggregates are formed as a result of surface cementation of acicular particle, which is aided by the Co^{2+} cations

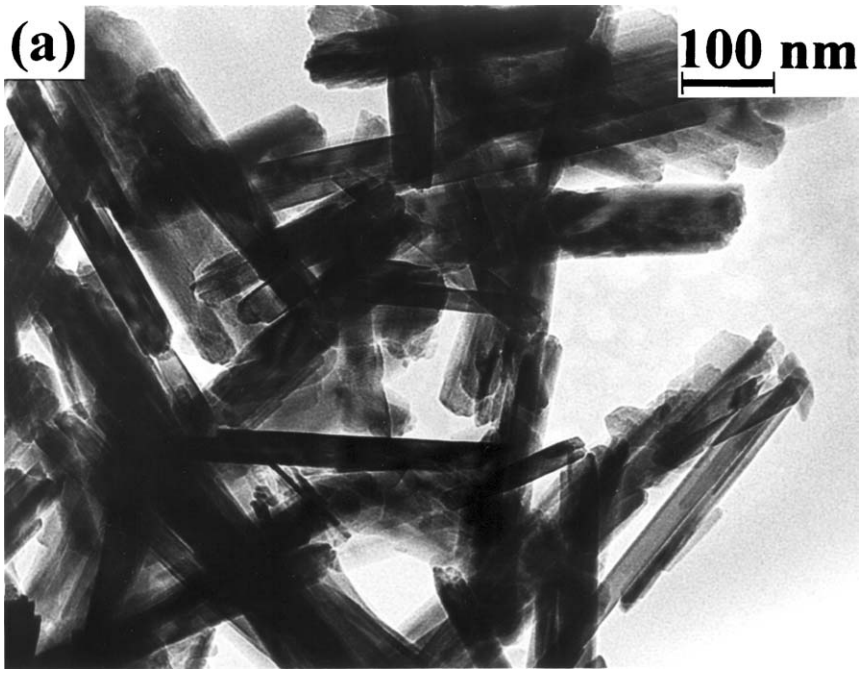

Figure 5 Electron micrograph of unsubstituted (HG) and Al^{3+}-substituted goethite for different at.% of Al^{3+} (a) HG, (b) HG-Al0.4, (c) HG-Al2, and (d) HG-Al 9. (*Continued*)

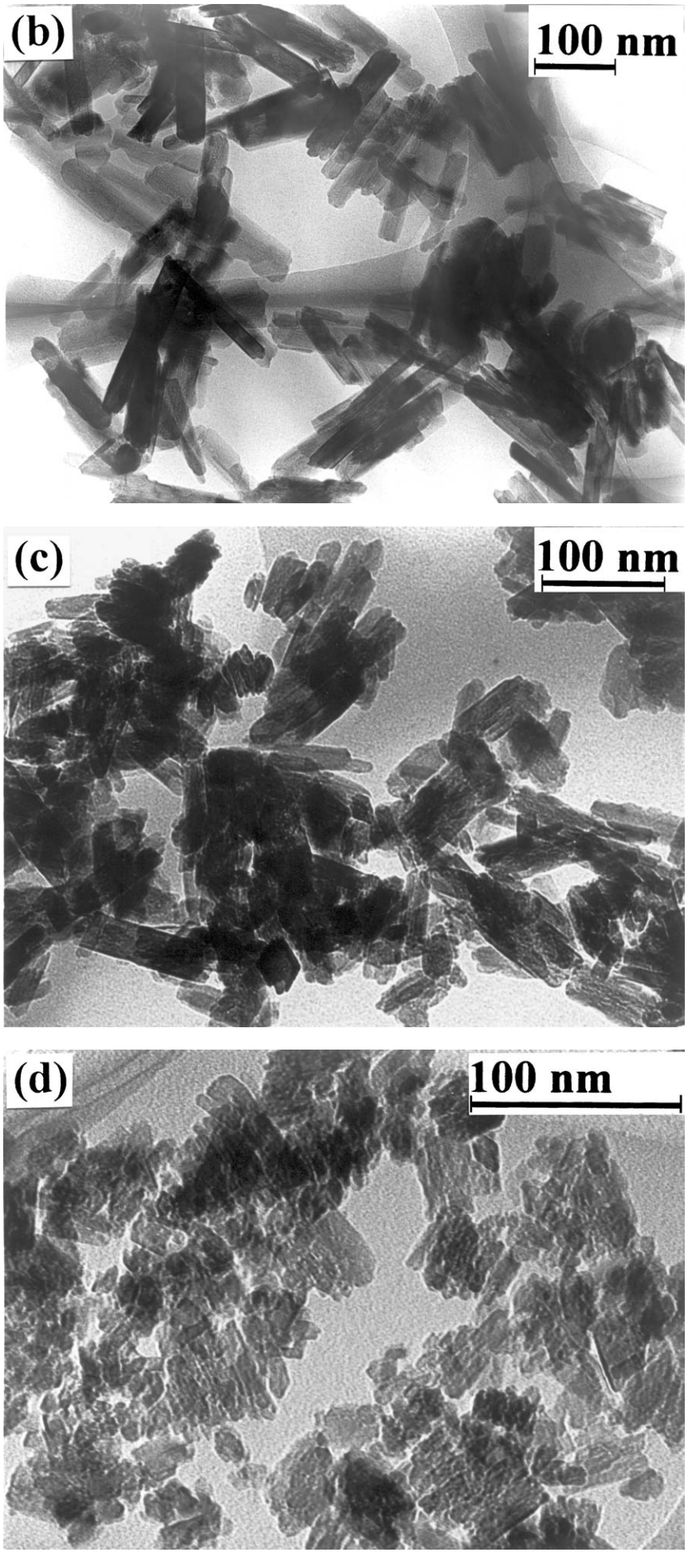

Figure 5 (*Continued*).

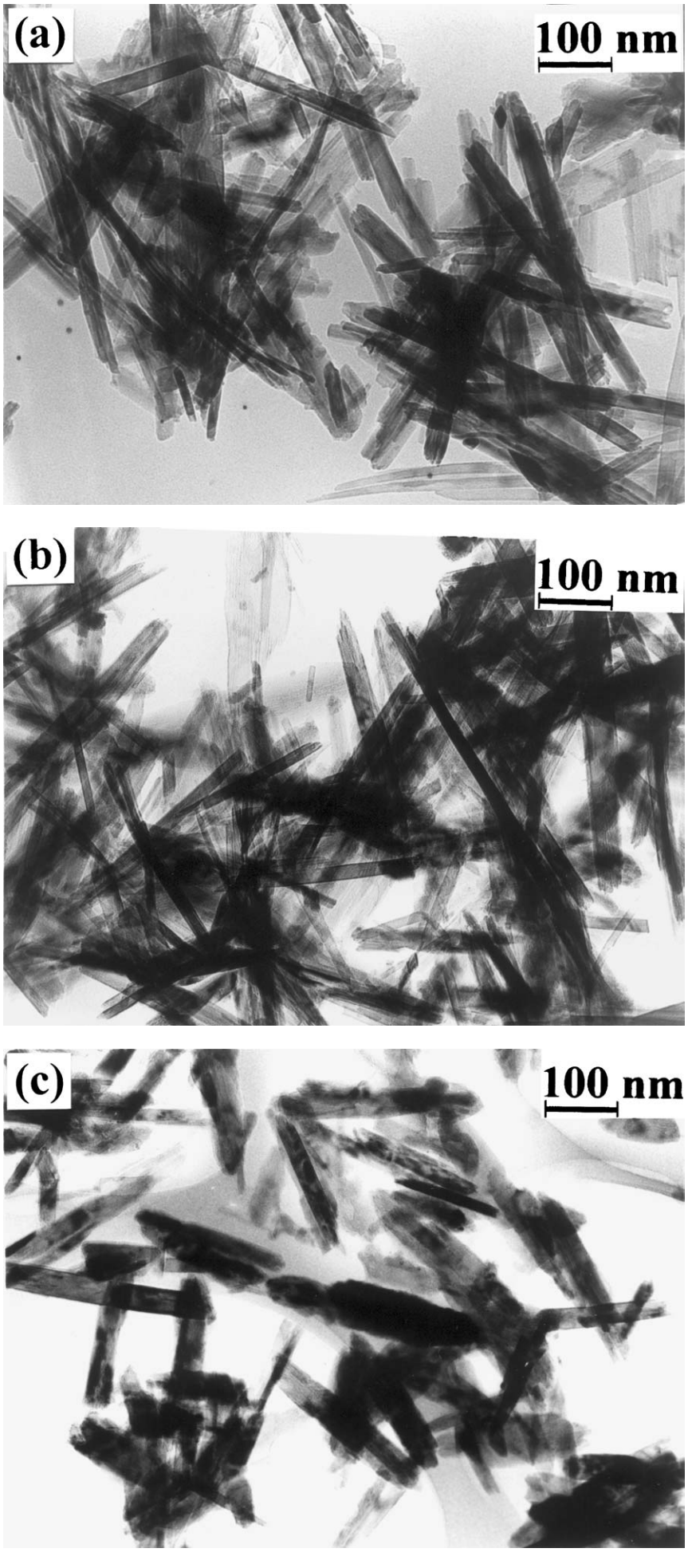

Figure 6 Electron micrograph of substituted goethite (a) HG-Co5, (b) HG-Co10, HG-Ni5, and (d) HG-Cr5. (*Continued*)

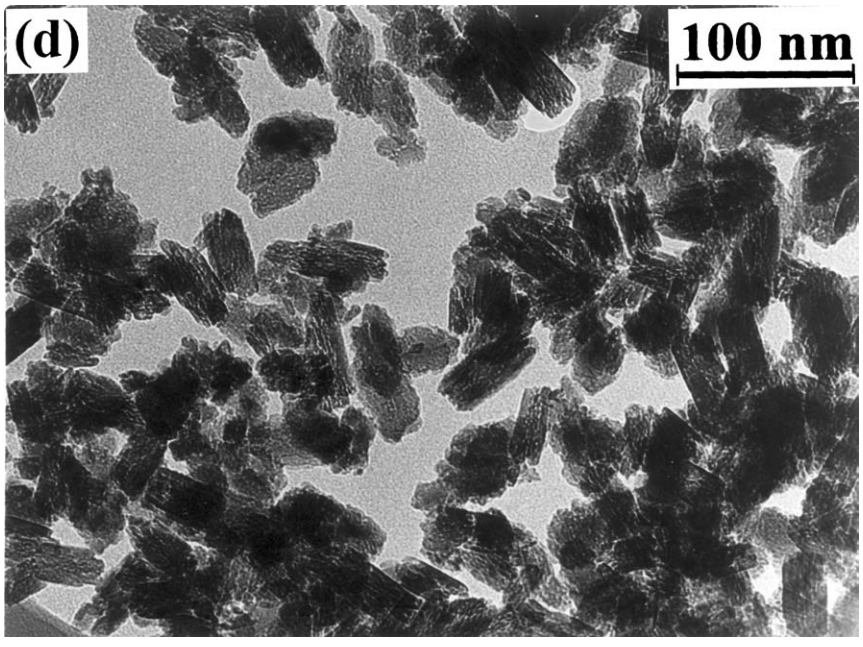

Figure 6 (*Continued*).

on the surface. The adsorption of impurities under high concentrations changes the surface charge, leading to aggregation. With Ni^{2+} substitution, the acicular particles do not show well-defined, (121)-type domal faces as observed in other cases. However the particle size and AR distribution remain unchanged as of unsubstituted HG samples. Tabular morphology of the particles is observed in Cr^{3+} as well as Al^{3+} (>1 at.%) substituted samples.

Maghemite phase is obtained by reduction followed by oxidation at 270°C. Fig. 8 shows the morphology of the resulting maghemite samples. The particles retain acicular morphology and incorporate near spherical pores of 5–15 nm (mesopores). The micrographs also show that some of the neighboring pores join together to form cylindrical mesopores. Interestingly, the particles do not disintegrate to smaller fragments even when their length is very small (in the case of ROHG-Al 9). Further, these particles remain single crystallites, as observed by spoty ED patterns, despite the discontinuity caused by the mesopores.

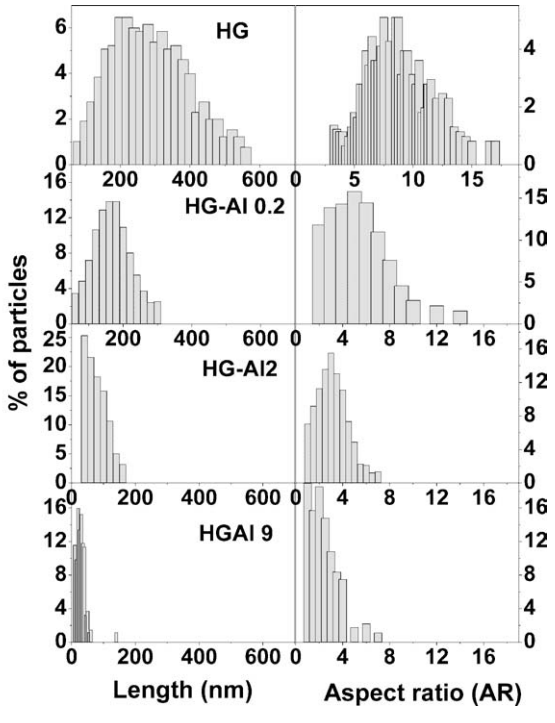

Figure 7 Histograms showing particle size and AR distribution of HG for different Al^{3+}at.%.

3.4. Infrared spectra studies

Infrared spectra of substituted goethite are shown in Fig. 9. They are similar to the IR spectra of α-FeOOH with additional absorption bands corresponding to water molecules indicating that the samples are to be better considered as hydrogoethite (HG). The peak assignments are given in Table III. The appearance of distinguishable shoulder at ~3400 cm^{-1} and absorption band at ~1640 cm^{-1} are characteristics of H─O─H stretching (hydrogen-bonded) and bending vibrations respectively. These bands reportedly arise from the strongly coordinated H_2O molecules present in strands of channels formed between the double ribbons of $Fe(O,OH)_6$ octahedra running parallel to *c*-axis in the goethite structure [7]. Absorption band around 3140 to 3180 cm^{-1} is due to O─H stretching mode of hydroxyl group. With substituted hydrogoethite, O─H stretching

TABLE II Length and Aspect ratio (AR) of substituted goethite

Substituent	Concentration (at.%)	Length (nm)	Aspect ratio
–	0	200–400	7–12
Al^{3+}	0.4	150–250	3–8
”	2	50–150	2–5
”	9	~50	2–3
Co^{2+}	5	200–400	7–25
”	10	200–400	7–25
Cr^{3+}	4.76	30–80	1–3
Ni^{2+}	4.76	150–350	4–9

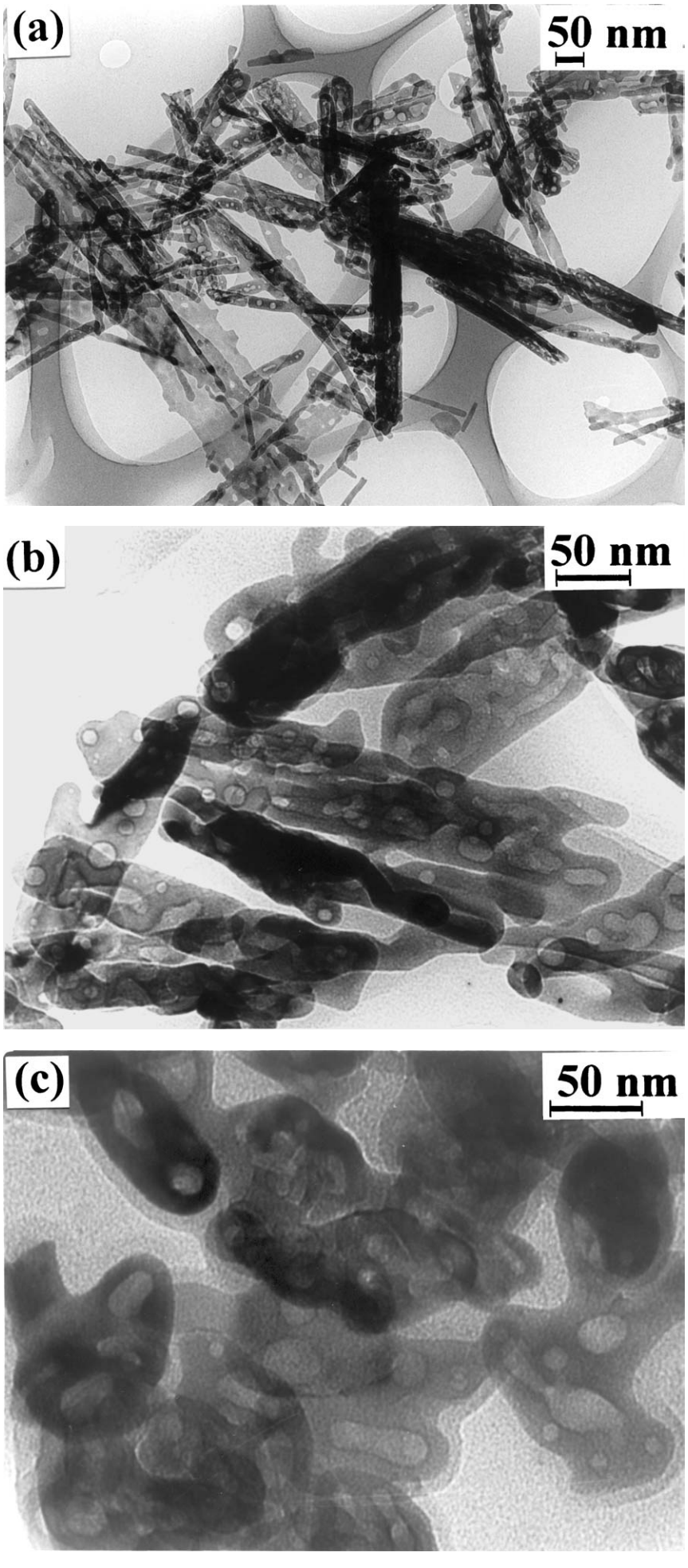

Figure 8 Electron micrographs of maghemite (a) ROHG-Co5, (b) ROHG-Al 0.4, (c) ROHG-Al2 and (d) ROHG-Cr5. (*Continued*)

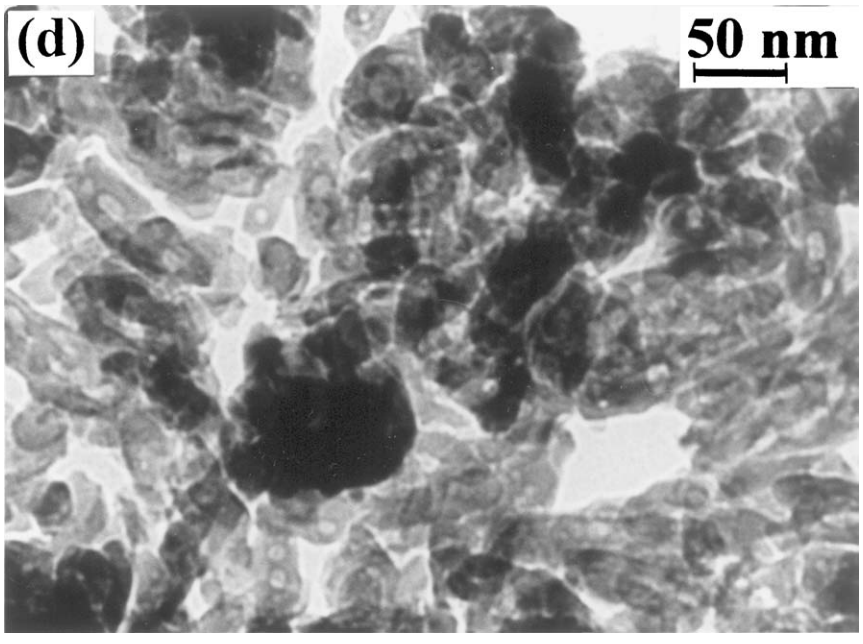

Figure 8 (*Continued*).

band shifts to higher frequencies. A direct correlation to the effect of substituents cannot be made on the ν_{O-H} stretching frequency. With increasing Al^{3+}, the O–H in-plane (δ_{O-H}) and out-of-plane (γ_{O-H}) bending bands shift to higher frequencies (Table III). However, absorption bands corresponding to Fe–O stretching shift to lower frequencies. Similar shifts in the absorption maxima are observed for Co^{3+}, Ni^{2+} and Cr^{3+} substituted HG. This indicated that the M–OH bond shortens with increasing concentration of the substituents. The shift in absorption bands is a clear evidence for the substitution of M^{n+} for Fe^{3+} taking place in hydrogoethite. Discernibly, broad, low intense peaks at around 1160 and 1120 cm^{-1} arise from minor fraction of lepidocrocite which was found to co-exist with HG-Co samples containing >8 at.% Co. However no

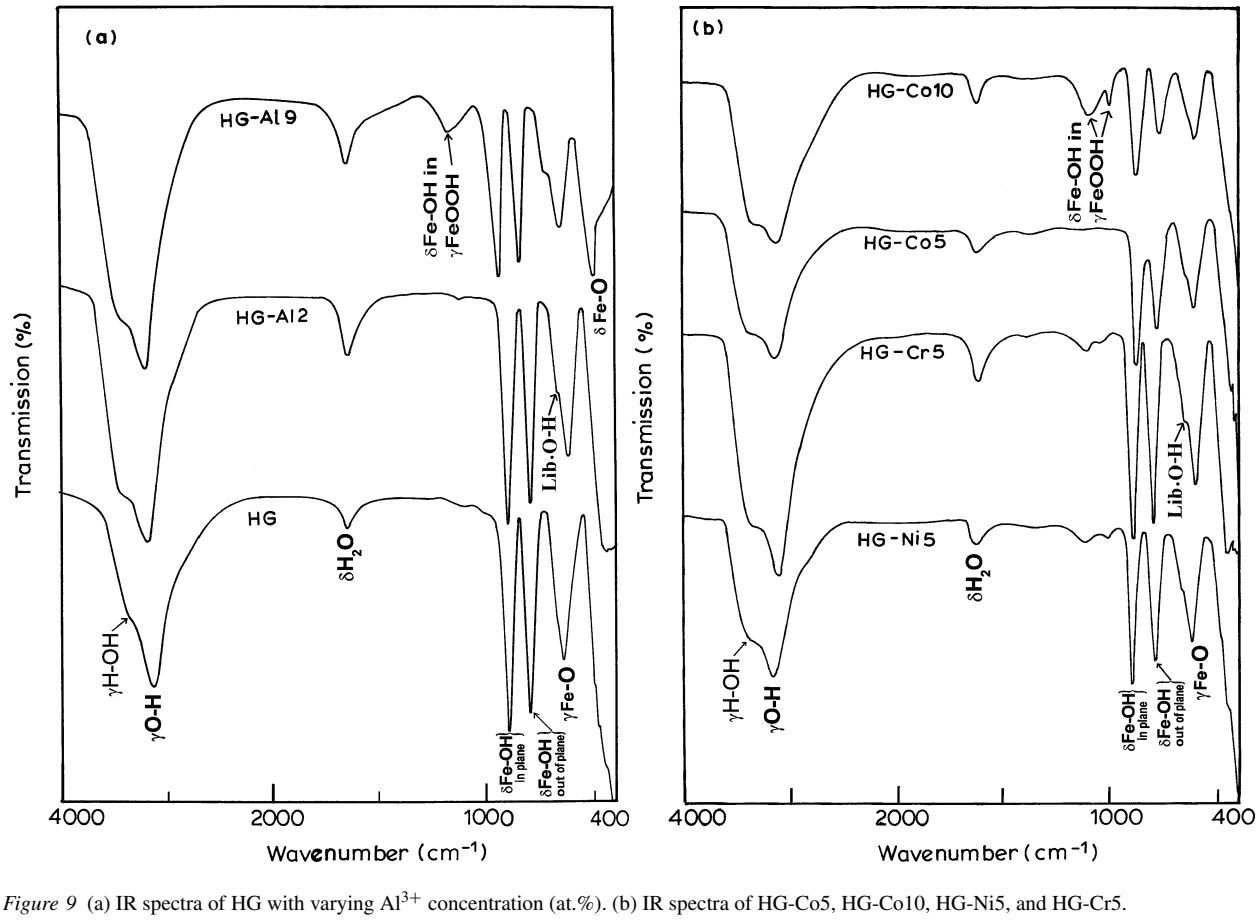

Figure 9 (a) IR spectra of HG with varying Al^{3+} concentration (at.%). (b) IR spectra of HG-Co5, HG-Co10, HG-Ni5, and HG-Cr5.

TABLE III Assignment of observed frequencies (cm^{-1}) in IR spectra of substituted goethite

Assignment	HG	HG-Al0.4	HG-Al2	HG-Al 9	HG-Co5	HG-Co10	HG-Ni5	HG-Cr5
H—O—H stretching	3400	3384	3384	3385	3414	3377	3385	3384
O—H stretching (νO—H)	3139	3147	3151	3141.5	3182	3178	3180	3150
H—O—H bending from H_2O	1652	1642	1636.3	1648.8	1638.2	1639.2	1630.5	1634.4
O—H bending from γ-FeOOH	–	–	–	1129.1	–	1124.3	1125.3	1127.2
O—H bending from γ-FeOOH	–	–	–	–	–	1021.1	–	–
O—H in-plane bend (δ_{O-H})	891.9	892.9	897.7	903.5	895.8	896.8	895.8	896.8
O—H out-of-plane bend (γ_{O-H})	795.5	796.5	799.4	803.2	798.4	798.4	795.5	801.3
OH^- librational mode	668.9	669.7	669	669.2	669.1	669.2	668.9	668.2
Fe—O stretch in FeOOH	635.4	633.4	621.9	614.2	633.5	631.6	625.8	621

detectable X-ray peaks of lepidocrocite were observed. Presence of highly crystalline, uniform particles are observed by TEM as well. Therefore, such absorption bands can only arise from intergrown regions of lepidocrocite in goethite. In fact, intergrown aggregate of acicular particles are observed in HG-Co10. Interestingly, the shoulder peak at 669 cm^{-1} arising from the librational (breathing) mode of OH^- group does not shift with substitution. This peak distinguishably emerges in the IR spectra, as Fe—O stretching shifts to lower frequency with the extent of cation substitution. IR absorption spectra reveal the presence of structurally coordinated lattice water in hydrogoethites.

3.5. Thermal analyses

Fig. 10a shows the simultaneous TG/DTA curves of Al^{3+}-substituted HG. There are two strong endothermic DTA peaks, the one at 265°C is accompanied by a shoulder around 250°C. The second endotherm appears at 300°C. With increasing Al^{3+} content, the two strong endotherms merge to appear as a broadened peak. Further, the shoulder endotherm (marked by arrows) persists without much shift around 250°C. This endotherm is accompanied by a weight loss from the release of strongly coordinated water of hydration in the interior of goethite crystallites. The observed weight loss was always greater than the theoretical weight loss in terms of the chemical formula, FeOOH (Table I). The merging of two strong endothermic peaks into a broad endotherm is due to the decrease in particle size, wherein the surface-related dehydration reaction is simultaneous to the dehydroxylation in the interiors. The weight loss is complete for all the Al^{3+}-substituted samples at $\leq$300°C, which is characteristic of crystalline particles of goethite.

In the case of Co- or Ni-substituted HG (Fig. 10b), two endotherms are observed. The first peak appears around 260°C and the second around 295°C. Whereas with Cr^{3+}-substituted HG only one broad endotherm

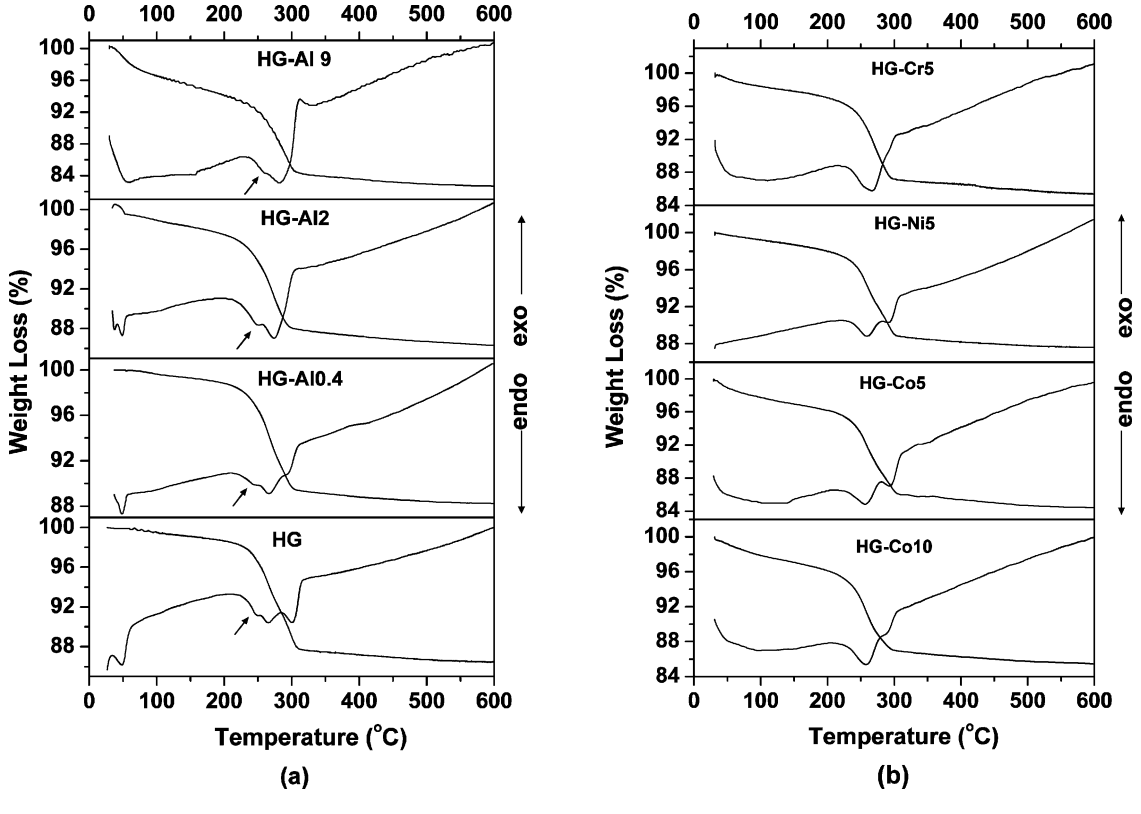

Figure 10 (a) TG/DTA curves of HG-Al samples with varying concentration of Al^{3+}(at.%). TG/DTA curves of HG-Co5, HG-Co10, HG-Ni5, and HG-Cr5.

exists at 265°C. There is no discernible shoulder endotherm in any case, because of the overlapping with the first endotherm. However, the shoulder endotherm is distinctly observed for Al^{3+}-substituted HG followed by strong endotherm around 265°C. With Cr^{3+}-substitution, the particle size goes down to 50 nm as also the aspect ratio to <3 and correspondingly the endotherm is broadened.

Isothermal weight loss measurements have also been carried out by heating the samples at selected temperatures. In all the cases, the weight-loss observed was more than the theoretical value for FeOOH although the samples were oven dried at 120°C for extended hours before measuring the isothermal weight-loss. The compositions of the substituted HG derived from the gravimetry (weight-loss) together with the Fe- contents determined by volumetric analyses are given in Table I. The differences between the isothermal and TG weight losses arise from the adsorbed water and are perceptible for samples with smaller particle size (<80 nm).

3.6. Magnetic measurements

Fig. 11 shows the M-H measurements for cation substituted maghemite samples recorded at room temperature. The magnetic properties such as saturation magnetization (σ_s) measured at 1T, coercivity (H_c) and squareness ratio as well as the pore shape and size of the particles are listed in Table IV. It is evident that the saturation magnetic moment, coercive field and hysteresis phenomenon depend strongly on the type of substitution in γ-$Fe_2O_{3-\delta}$. In all the samples, cylindrical mesopores are formed within each particle. The changes observed in σ_s and H_c are also affected by the shape and size of the particles, apart from the substitutional effects. Fig. 12 shows the variation of σ_s and H_c with the concentration of substituents. σ_s decreases considerably with increasing Al^{3+}, Cr^{3+}, Co^{2+} or Ni^{2+} in maghemite. The decrease in magnetic properties is more conspicuous with the substitution of diamagnetic cations (e.g. Al^{3+}) and less with the substitution of transition metal ions. Substituents, irrespective of the charge, are reported to prefer the octahedral (B site) sublattice in magnetite [12]. Thus, the effective magnetic moment giving rise to the net magnetization decreases with the substitution of diamagnetic cations. Whereas on substituting Co^{2+}, Cr^{3+} or Ni^{2+} (where effective magnetic moment is <5 μ_B), σ_s decreases only marginally. Smaller size of the particles with high surface area lowers σ_s due to relaxation effects of spins of magnetic atoms located around the surface region. By way of comparison, notwithstanding the particle shape and size remaining nearly the same, σ_s (52.1 emu/g) and H_c (93.92 Oe) for ROHG-Al 9 are relatively low compared to σ_s (62.9 emu/g) and H_c (151.3 Oe) for ROHG-Cr5. The coercivity decreases with substitution except for RO-HG-Co samples, with 5 and 10 at.% of Co, the H_c values are 575 and 610 Oe respectively.

TABLE IV Magnetic properties of γ-$Fe_2O_{3-\delta}$

γ-$Fe_2O_{3-\delta}$	σ_s at (10 KOe)/emu g^{-1}	Coercivity H_c/Oe	Squareness ratio
ROHG	74.38	319.3	0.45
ROHG-Co5	63.81	574.9	0.509
ROHG-Co10	59.96	608.8	0.44
ROHG-Al0.4	72.5	310.8	0.42
ROHG-Al2	65.4	140.9	0.27
ROHG-Al 9	52.1	93.92	0.226
ROHG-Cr5	62.9	151.3	0.28
ROHG-Ni5	66.6	285.8	0.42

3.7. Mössbauer spectroscopy

The ^{57}Fe Mössbauer spectra of maghemite samples are recorded at room temperature in the transmission geometry by using a source of ^{57}Co in Rh matrix in constant accelerating regime. Isomer shifts were referred to with respect to natural iron. The spectra were fitted by computing upto six sextets, in addition to a doublet

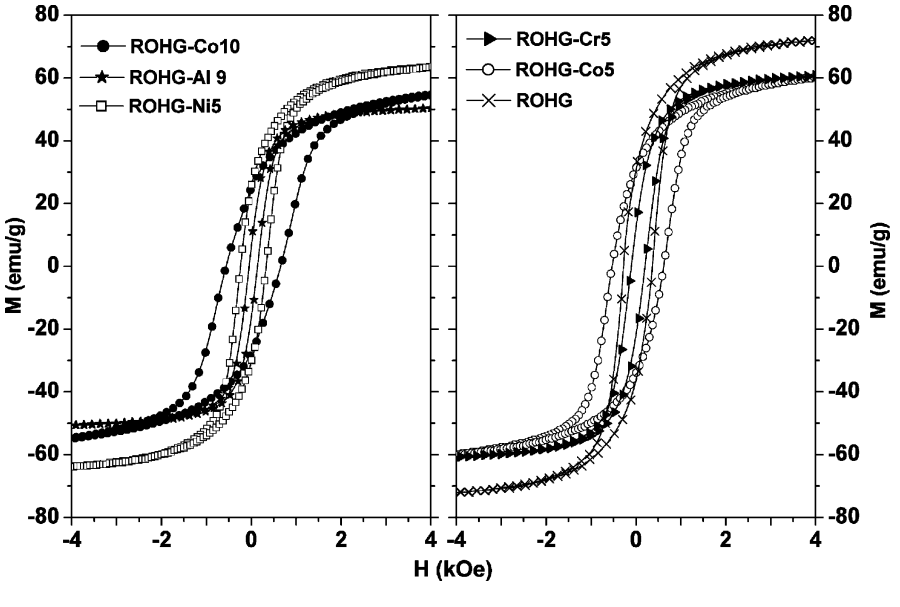

Figure 11 B-H curves of maghemite derived from substituted goethite.

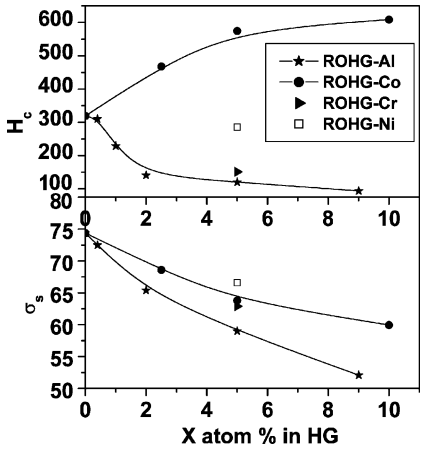

Figure 12 Change in σ_s and H_c with varying concentration of substitution.

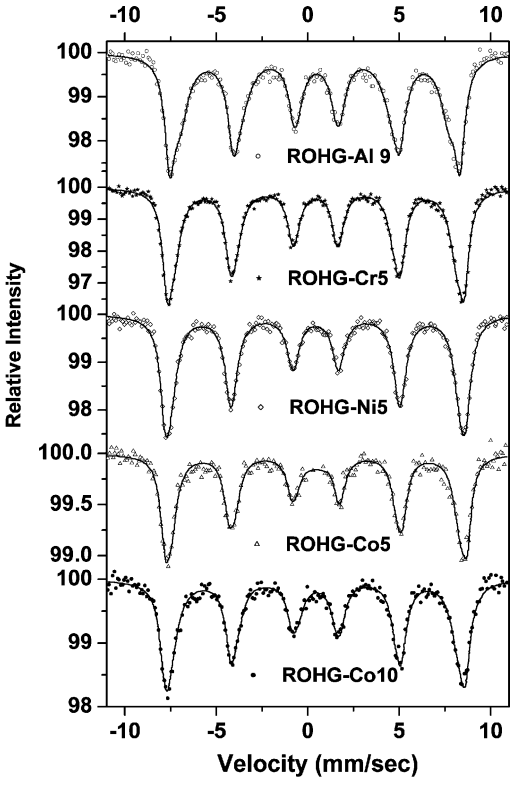

Figure 13 Mössbauer spectra of maghemite derived from substituted goethite.

and singlet generally attributable to the different phases possibly present in the samples. The Mössbauer spectra of all the samples showed the presence of only magnetically ordered components. No asymmetric doublets corresponding to the superparamagnetic state of the particles are observed. This clearly indicates, despite the smaller width of particles along with the mesopores, that magnetic ordering is prevailing strong. Typical cases of Mössbauer spectra of γ-$Fe_2O_{3-\delta}$ for the samples ROHG-Mx; M = Co, Ni, Cr or Al with $x = 5$ or 10 at.%, are shown in Fig. 13. Iron in its trivalent state is inferred from the isomer shift. Near zero values of quadrupole splitting (QS) for the sextets reveal the defect spinel structure characteristic of all the samples. However broadened linewidth of the absorption peaks are clearly decipherable from Fig. 13, indicating the changes in distribution of hyperfine interaction field (Table V). Such distribution can arise as result of smaller particle sizes with large number of Fe^{3+} ions at or near the surface. Accordingly the effective magnetic field calculated from the fitted spectral data, assuming lines to be Lorentzian in shape shows two sextets and the values are given in Table V. In all the samples, other- than ROHG-Al 9, H_{eff} for sextet-I showed hyperfine interaction of bulk ferrimagnetic γ-$Fe_2O_{3-\delta}$, corresponding to Fe^{3+} ions situated in the core of the nanoparticles. The effect of substitution had shown minor changes in H_{eff} from ROHG. Detectable decrease is seen in ROHG-Al 9, where the presence of diamagnetic Al^{3+} in octahedral sites brings down H_{eff} to a low value of 492 kOe. This clearly shows the homogeneous distribution of the substituents in maghemite. The origin of the magnetic hyperfine field in iron oxides is the polarization of the inner 's' electrons of the atoms by the Fe 3d electrons. Minor contribution also comes from the polarization of the 's' electrons by the neighboring cations and from the spin dipolar moment of the 3d electron themselves. Therefore, H_{eff} decreases as diamagnetic cations such as Al^{3+} enter the structure. This can be explained on the basis of a supertransfer mechanism. As the number of Al-O-Fe paths increases, the supertransfer of 3d-spin density into the outer 's' shell of the iron nuclei, and hence the total hyperfine field, decreases [13]. Similarly, H_{eff} from sextet-II of

TABLE V Mössbauer parameters of γ-$Fe_2O_{3-\delta}$

Sample ID	Sextet	Isomer shift δ/mm s^{-1}	Quadrupole splitting ΔE_q/mm s^{-1}	Line width /mm s^{-1}	Hyperfine field H_{eff}/T	Area (%)
ROHG	I	0.34	0.01	0.54	503	78.3
	II	0.31	−0.07	0.59	492	21.7
ROHG-Cr5	I	0.32	0.00	0.59	504	53.5
	II	0.34	−0.01	0.97	480	46.5
ROHG-Al 9	I	0.35	−0.05	0.62	492	47.1
	II	0.33	−0.5	1.13	457	52.9
ROHG-Ni5	I	0.32	0.01	0.68	508	58.5
	II	0.33	−0.01	0.85	488	41.5
ROHG-Co5	I	0.34	0.01	0.51	514	63.2
	II	0.36	−0.02	0.89	494	36.8
ROHG-Co10	I	0.34	−0.02	0.67	507	57.1
	II	0.35	−0.06	1.06	486	42.9

the samples showed a decrease in effective hyperfine interaction. The smaller H_{eff} value as compared to bulk γ-$Fe_2O_{3-\delta}$ is due to the small particle size and can be associated with Fe^{3+} ions at or near the surface. The decrease was more pronounced with ROHG-Al 9 with $H_{\text{eff}} = 457$ kOe, as a result of the combined effect of increased Al-O-Fe paths and the smaller particle size whereby a large portion of Fe^{3+} ions reside on the surface of the particles. Further, the area under the sextet-I and sextet-II clearly shows the effective contribution from the core and surface atoms respectively. Thus, for ROHG-Al 9 and ROHG-Cr5, where the particle size is low, the area under sextet-I and sextet-II are almost equal. Whereas, for ROHG, the area under sextet-I (78.3%) is larger compared to the area under sextet-II (21.7%). As a result of nanosize of the particles considerable contribution prevails from the surface-located Fe^{3+} ions, leading to the line broadening.

4. Discussion

Substituted goethite particles with different size and shape are prepared from aqueous suspensions of FAS and M^{n+} salt (sulphate) solutions. The process of formation of goethite from $Fe(OH)_2 \cdot xH_2O$ by air oxidation is studied in detail in [7]. In fact, growth of goethite particles proceeds by the oxidation of $Fe(OH)_2 \cdot xH_2O$ to an intermediate phase through the nucleation within the amorphous ferric oxy-hydroxide. Thus, goethite evolves by heterogeneous nucleation and growth process [8]. However, the substituents influenced tremendously the particle size as well as the aspect ratio in comparison to the corresponding features of unsubstituted goethite. The isovalent substituents in FeOOH occupy the octahedral positions within the oxygen framework leading to isostructural solid solutions with AlOOH, CrOOH, etc. The substituted cations do not modify the goethite structure as evidenced from XRD; but they do affect the size of the unit cell. However the goethite crystallites become smaller as Al^{3+}-substitution increases. Throughout the range of concentration of the substituents attempted, the particles remained monocrystallites.

Dehydoxylation of the particles takes place in the narrow range of temperature (250–300°C) in all the samples as evidenced from the TG/DTA analysis, indicating the complete crystallinity of the samples, in spite of the varying particle size. The shift of O–H stretch to lower frequencies, accompanied by the change in M–O–H bending vibration to higher frequencies with Al^{3+} substituting for Fe^{3+}, indicates the increase in the hydrogen bond strength. It is reported that due to the loss in crystallinity, O–H stretching frequency increases and bending vibrations decreases in goethite [14]. The change in shape and size of the crystallites may be associated with the increased nucleation rate and restricted growth along the c-axis as Al^{3+} concentration increases. Diaspore (α-AlOOH) and goethite (α-FeOOH) are compounds based on orthorhombic lattice with space group Pbnm, with the lattice parameters: $a = 4.40$ Å, $b = 9.43$ Å, and $c = 2.84$ Å for α-AlOOH [15] and $a = 4.58$ Å, $b = 9.937$ Å, and $c = 3.015$ Å for α-FeOOH [10]. Despite the isomorphous structure of goethite with diaspore, Al^{3+} can replace only one-third of the Fe^{3+} in synthetic goethite, whereas upto half of Fe^{3+} substitution is found to exist in natural goethite [6]. The increasing strain in the crystal structure due to the size mismatch and limited contractibility of oxygen octahedra of Fe are attributed as the primary reasons for Al substitution being restricted to <0.33 [16]. The substitution, however, shows severe effect on the particle shape and size, because of the anisotropy in the growth rate and the strain induced in the lattice. The lattice of diaspore is 14.25% smaller than that of goethite. Anisotropic growth rate results from the octahedral arrangements as well as from the strength of the hydrogen bond across the double chains of octahedra. The goethite structure is built from double bands of octahedra running parallel to the crystallographic c-axis. The octahedral double bands are linked by shared oxygen along their edges and also by hydrogen bonds that bridge the gaps between the atomic double bands within the structure [17]. Thus, in general, growth along the c-axis is faster where the edge sharing $Fe(O,OH)_6$ octahedra are arranged as strands of double chains. Along a- and b-axes, the growth rate is predominantly governed by the strength of hydrogen bond, which is stronger in AlOOH compared to FeOOH. Hydrogen bond in AlOOH has the strongest vector along the crystallographic a-direction, whereby the growth along this direction is relatively faster giving rise to tabular particles of diaspore, whereas for goethite, the particles remain acicular in morphology. Further, during the growth of the double chains of iron in octahedral oxygen coordination, i.e. $Fe(O,OH)_6$, along c-axis the substitution of $Al(O,OH)_6$ in between $Fe(O,OH)_6$ octahedra will introduce lattice strain, which increases with Al^{3+} concentration, inhibiting the progressive growth along the c-axis. The tendency to have shorter lengths in HG-Alx particles also can be understood from the natural crystal morphology of diaspore (α-AlOOH) in comparison to that of goethite (α-FeOOH). Diaspore has tabular morphology, whereas, goethite is acicular. Thus, with increasing concentration of Al^{3+}, acicular goethite tend to acquire shorter length, thereby, AR decreases. Similar effects on the particle size and AR are observed with Cr^{3+}-substituted samples. α-CrOOH (bracewellite) has orthorhombic lattice with space group Pbnm, with the lattice parameters: $a = 4.492$ Å, $b = 9.86$ Å, and $c = 2.974$ Å (JCPDS 25-2497). These values lie in-between those of goethite and diaspore. HG-Cr5 and HG-Al 9 samples compare in particle size. However, the former is more uniform in size and lath-shaped.

In addition to M^{3+} cations, M^{2+} ions also enter Fe^{3+} position in FeOOH. It is reported that apart from the ionic radius, the contributions from the substitutional cation to the change in lattice energy is considered to influence the tendency of such cations to replace Fe^{3+} in iron oxide/oxyhydroxide [18]. It is reported that the incorporation of Co^{2+} into the goethite structure is preceded by the oxidation of the ion to the trivalent form. With Co-substitution, the particles are slender with the width of 20–30 nm and AR as high as 25. Thus, Co- limits the growth of the particle perpendicular to the

a-axis, which is identified as [100] from the ED pattern, forming the width of the particle. The particles are made up of well-defined domal planes. Whereas, HG-Ni5 exhibit nearly the same size and shape as that of unsubstituted HG. The particles however show nonuniform edges along the *c*-axis. This can be due to the preferential substitution of Co- and Ni-ion on different crystallographic directions when the nuclei of oxyhydroxide grow from the amorphous phase. Incorporation of M^{2+} in hydrogoethite is preceded by the coprecipitation of M^{2+} ion along with the $Fe(OH)_2 \cdot xH_2O$ gel. During growth by heterogeneous nucleation from the gel, Co^{2+} may get easily incorporated in the octahedral sites of FeOOH structure preceded by the oxidation of Co^{2+} to Co^{3+}, as the ionic radius is close to that of Fe^{3+}. The crystallites grow by constructing the edge sharing octahedra along the *c*-axis. Perpendicular to *c*-axis, the growth can be restricted by several factors; growth anisotropy, development of anionic defect and diminished amount of bridging H_2O which may give rise to low bonding strength between the double chains running along the *c*-axis. In the case of Ni^{2+}, the substitution along *c*-direction may be difficult due to larger ionic radius of Ni^{2+}. A maximum incorporation of <6 mol% of Ni^{2+} has been reported in goethite structure [19]. The non-uniform edges of the particle with acicular shape thus reflect the Ni^{2+} incorporation in the goethite structure, which brings about the distortion in the domal planes. With increasing concentration of substituents (at different levels for various substituents) secondary phases such as γ-FeOOH, $M^{n+}(OH)_n$ or spinel ferrites form at trace levels. Thus, with higher concentrations of Al^{3+} (>10 at.%) and Cr^{3+} (>5 at.%) substitutions, traces of lepidocrocite were observed. Whereas, Co- substitution above 10 at.% give rise to lepidocrocite phase which can be detectable from IR spectra. While with Ni^{2+}, at >5 at.% gives presence of amorphous phase of $Ni(OH)_2$ or $NiFe_2O_4$.

Maghemite derived from substituted goethite showed substantial differences in magnetic properties depending upon the particle size, shape and substituents. With Al^{3+} substitution, AR and particle size decreases and coercivity goes down to very low values (<100 Oe). Change in σ_s is also observed as a result of the increased surface area of smaller size particles, where the relaxation of spins lying on the surface of the particles contributes largely to the effective magnetization. Decrease in coercivity is enhanced by the presence of diamagnetic ion (Al^{3+}). Whereas, transition metal ion substituents (with definite magnetic moment) in maghemite also showed dependence in H_c with particle size and AR. Further, in Co-substituted maghemite, presence of homogeneously distributed Co^{2+} ions enhances the magnetocrystalline anisotropy, thereby increasing H_c. The anisotropy constant and anisotropy field for $CoFe_2O_4$ is much higher compared to other spinel ferrites [20]. Whereas for all the other samples of substituted maghemite (where the AR of the particles is low), in addition to the low magnetocrystalline anisotropy, the shape anisotropy decreases and H_c diminishes to levels lower than that of the unsubstituted maghemite. For ROHG-Co samples, the magnetization vector remains within the long axis due to shape-anisotropy and coincides with the magnetocrystalline anisotropy. Therefore, these two properties behave additively, giving rise to high magnetic anisotropy which, in turn, increases the coercivity of the particle. It is known that addition of small quantities of Co^{2+} to γ-$Fe_2O_{3-\delta}$ particles results in stronger coercive field (~400 Oe) [21, 22]. The so-called Co-modified γ-Fe_2O_3 or co-adsorbed γ-Fe_2O_3 is obtained at relatively low temperatures ($T < 150^\circ$C). The deposition of a Co-rich surface layer results in the increase of coercive field due to the formation of uniaxial anisotropy. When Co is made to diffuse through the maghemite particle at high temperatures ($T > 300^\circ$C), the Co-doped γ-Fe_2O_3 (where the composition is close to $CoFe_2O_4$) has higher H_c due to increase in magnetocrystalline anisotropy. However the high temperature processing of these particles causes splitting of the particles to shorter lengths. Further, partial conversion of γ-Fe_2O_3 to α-Fe_2O_3 takes place during high temperature heating. For γ-$Fe_2O_{3-\delta}$ magnetic particles with 10% cobalt ferrite on the surface, the coercivity is around 600 Oe [23]. Such particles find application as high-density recording materials. Whereas, the present method can be used as a single step method for the preparation of Co-substituted maghemite with better magnetic properties instead of the commonly employed two step process, namely the derivation of maghemite from the precursor and the epitaxial coating of cobalt ferrite on maghemite particles. However, the introduction of Co in the precursors has been a problem where the shape is not controllable. The present results clearly depict the simplicity of the wet chemical methods in the formation of substituted acicular HG and the optimum magnetic properties of maghemite derived from it. In order to further increase H_c for the currently developing high-density recording materials, dopants such as Mn has to be employed along with Co as was the case reported for Co- and Mn- doped nonacicular γ-$Fe_2O_{3-\delta}$ which possess high coercivity of upto 2150 Oe [24].

5. Conclusions

The process of formation of goethite with varying aspect ratio is realized by the cationic substitution as much as by controlling the processing conditions. Further, the magnetic properties of γ-$Fe_2O_{3-\delta}$ derived from such carefully prepared precursors have to be studied for its desirable applications such as magnetic fluids, magnetic recording media, etc. The present study provides the effect of cations (Al^{3+}, Co^{2+}, Cr^{3+} and Ni^{2+}) on the particle shape and size of goethite. While Al^{3+} and Cr^{3+} showed decreasing AR (<4) with increasing concentration, Co-substitution increased the AR (>25) of the particles. The magnetic property of maghemite derived from substituted goethite showed dependence on the particle shape, size and concentration of the substitution. Lower σ_s and H_c are observed for particles with low aspect ratio, size and large concentration of diamagnetic ions. Higher coercivity was obtained with Co-substituted γ-$Fe_2O_{3-\delta}$ due to increase in magnetocrystalline anisotropy. Single step processing of

Co-substituted γ-$Fe_2O_{3-\delta}$ particles having equally good magnetic properties, as that of two-step processing of Co-coated γ-$Fe_2O_{3-\delta}$ is advantageous by way of economy and time saving process.

Acknowledgement

The Board of Smart Materials Research and Technology of NPSM, Government of India, is acknowledged for the research funding.

References

1. J. H. ADAIR and E. SUVACI, *Current Opinion in Colloid and Interface Sci.* **5** (2000) 160.
2. R. DAGANI, *Chem. Eng. News* **23** (1992) 18.
3. G. BATE, in "Ferromagnetic Materials," edited by E. P. Wohlfarth (North-Hollond, 1980) Vol. 2, Chap. 7.
4. H. HIBST and E. SCHWAB, in "Materials Science and Technology," edited by R. W. Cahn, P. Hassen, and E. J. Kramer (VCH, Weinheim, 1994) Vol. 3B, p. 212.
5. U. SCHWERTMANN, U. GASSER and H. STICHER, *Geochimica et Cosmochimica Acta* **53** (1989) 1293.
6. R. M. CORNELL and U. SCHWERTMANN, in "The Iron Oxides" (Wiley-VCH, Weinheim, 1996).
7. C. SUDAKAR, G. N. SUBBANNA and T. R. N. KUTTY, *J. Mater. Chem.* **12** (2002) 107.
8. G. N. SUBBANNA, C. SUDAKAR and T. R. N. KUTTY, *Mater. Chem. Phys.* **78** (2002) 43.
9. E. VON MEERWALL, *Comput. Phys. Commun.* **9** (1975) 117.
10. A. F. GUALTIERI and P. VENTURELLI, *American Minerologist* **84** (1999) 890.
11. F. D. BLOSS, in "Crystallography and Crystal Chemistry: An Introduction" (Holt, Rinehart and Winston, Inc. Newyork, 1971).
12. M. SORESCU, D. M. TARABASANU and L. DIAMANDESCU, *Appl. Phys. Lett.* **72**(16) (1998) 2047.
13. E. DE GRAVE, G. M. DA COSTA, L. H BOWEN, U. SCHWERTMANN and R. E. VANDERBERGHE, *Clays and Clay Minerals* **44** (1996) 214.
14. E. HARTERT and O. GLEMSER, *A. Elektrochemie* **60** (1956) 746.
15. H. D. MEGAW, in "Crystal Structures: A Working Approach" (W.B. Saunders company, London, 1973)
16. A. C. SCHEINOST, D. G. SCHULZE and U. SCHWERTMANN, *Clays and Clay Minerals* **47**(2) (1999) 156.
17. L. BRAGG and G. F. CLARINGBULL, in "Crystal Structures of Minerals" (G Bell and Sons, 1965).
18. B. S. W. DAWSON, J. E. FERGUSSEN, A. S. CAMPBELL and E. J. B. CUTLER, *Geoderma* **35** (1985) 127.
19. J. GERTH, *Geochimica et Cosmochimica Acta* **54** (1990) 363.
20. J. SMITH and H. P. WIJN, in "Ferrites" (Philips Tech. Library, 1959).
21. R. VALENZUELA, in "Magnetic Ceramics" (Cambridge University Press, 1994).
22. E. SCHWAB and R. J. VEITCH, *IEEE Trans on MAG.* **24**(2) (1988) 1883.
23. K. SUMIYA and T. MATSUMOTO, *J. Phys. Chem. Solids* **40** (1979) 1097.
24. M. C. DEND and T. S. CHIN, *Jpn. J. Appl. Phys.* **30** (1991) L1276.

Received 28 August 2002
and accepted 31 March 2004